NANO LETTERS

2007
Vol. 7, No. 2
276−280

Rings of Single-Walled Carbon Nanotubes: Molecular-Template Directed Assembly and Monte Carlo Modeling

Shengli Zou, Daniel Maspoch, Yuhuang Wang, Chad A. Mirkin,* and George C. Schatz*

Department of Chemistry and International Institute for Nanotechnology, Northwestern University, 2145 Sheridan Road, Evanston, Illinois 60208-3113

Received September 25, 2006; Revised Manuscript Received December 20, 2006

ABSTRACT

Rings of single-walled carbon nanotubes (SWNTs) were assembled by dip-pen nanolithography (DPN) generated molecular templates consisting of COOH-terminated monolayers in circular patterns surrounded by passivating CH_3-terminated SAMs. Experimental data and atomic-level Monte Carlo simulations show that SWNTs assemble into rings with radii as small as 100 nm at the edge of the COOH templates. This directed assembly is strongly length-dependent; only when the length of a SWNT is longer than half of the circumference of the circle does the SWNT bend to precisely follow the interface of the COOH-terminated monolayer. The theoretical modeling shows that the strain energy of each SWNT is balanced by the energy difference between the van der Waals interactions of the tube with COOH and CH_3 templates to produce the resulting ring structure.

The assembly and manipulation of nanoscale building blocks[1−6] are among the most important scientific challenges in nanoscience[7] because they not only afford a potential route to the fabrication of large-scale integrated nanoscale devices[8−11] but also provide a better understanding of the issues that govern self-organization in many classes of materials.[12] We have recently developed a directed assembly approach for positioning and shaping single-wall carbon nanotubes (SWNTs) into rationally designed structures based upon their interaction with nanopatterned monolayer templates.[13] Here the SWNTs are assembled along the boundary between hydrophilic and hydrophobic molecule-based features that are deposited on a gold substrate using dip-pen nanolithography (DPN),[14,15] allowing one to manipulate and assemble the SWNTs on the micrometer to sub-100-nm length scales. Thus, for example, SWNT rings can be formed on circular features of 16-mercaptohexadecanoic acid (MHA) that are surrounded by a passivating layer of 1-octadecanethiol (ODT).

SWNT rings have been fabricated by other procedures, beginning with the work of Liu et al., who obtained them as a low-yield byproduct in nanotube synthesis.[16] Soon after, Avouris and co-workers obtained SWNT rings that were stabilized by sidewall−sidewall van der Waals (VDW) interactions.[17,18] They proposed that the ring structures are formed at a bubble−liquid interface. Later, Sano et al. synthesized SWNT rings from end-functionalized tubes by a ring-closure reaction.[19] More recently, Tsukruk et al. have fabricated bent SWNTs, a close kin to the rings, on a silicon surface by trapping the SWNTs at liquid−solid−vapor contact lines.[20] The SWNT rings formed using these processes typically have diameters over 500 nm. Rings with diameters as small as 120 nm were obtained only recently by Xie's group using a chemical vapor deposition technique.[21] The unusual curvature-dependent electronic and magnetic properties of these SWNT ring structures have attracted a great deal of interest over the past several years.[22]

Differing from these previous studies, our method is built upon molecular-template directed assembly methods[23,24] and allows one to make SWNT rings with specified diameters on a surface. This SWNT assembly is driven by the dewetting of solvents over patterned hydrophobic/hydrophilic monolayers as well as by strong VDW interactions between SWNTs and COOH-terminated self-assembled monolayers (SAMs).[13] However, the length scale, which governs the formation of SWNT rings on a surface, and the minimum radius of fabricated rings one can obtain via this procedure are still undetermined. In this letter, we report the formation of SWNT rings with radii as small as 100 nm along with

* Corresponding authors: Tel: (+1) 847-491-5657 (G.C.S.); (+1)847-491-2907 (C.A.M.). Fax: (+1) 847-491-7713 (G.C.S.); (+1)847-467-5123 (C.A.M.). E-mail: schatz@chem.northwestern.edu; chadnano@northwestern.edu.

10.1021/nl062258e CCC: $37.00
Published on Web 01/06/2007

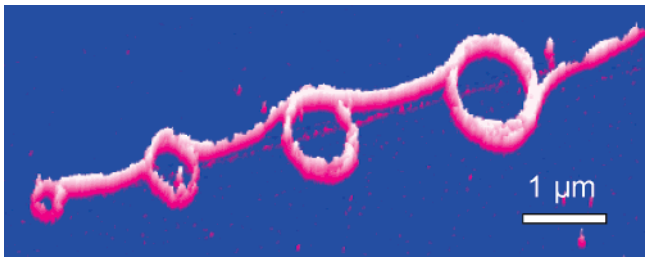

Figure 1. 3D AFM tapping-mode topographic image of a series of SWNT rings with diameters of 300 nm, 600 nm, 900 nm, and 1.1 μm. The image was taken at a scan rate of 0.5 Hz. The height scale is 30 nm.

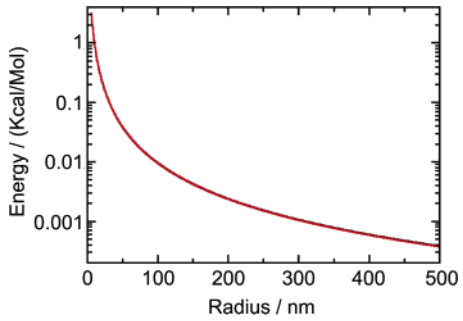

Figure 2. Evolution of the energy of a SWNT ring (per carbon atom) as a function of the radius of the tube arc, based on an idealized circular model of the tube structure.

atomic-level Monte Carlo simulations that show the required conditions for bending the SWNTs to form rings or arcs. The data show that this is a versatile way for controlling the bending of the SWNTs on a surface and the diameters of the resulting ring structures (Figure 1).

The forces that lead to SWNT ring formation involve a balance between nanotube strain and the difference in VDW interactions between the SWNT and the COOH- and CH_3-teminated monolayers. The maximum bending of the assembled SWNT rings can be predicted by simply calculating these two balancing forces. Consider for example the strain energy of a bent SWNT (assumed to be a portion of a circular arc) as a function of its radius. A 10-nm-long (9,6) SWNT, constructed of 1221 atoms, was used in these calculations. The carbon atoms were treated as aromatic sp^2 carbons with equilibrium bond lengths of 1.400 Å and bond angles of 120°. The strain of the SWNT is described using the Amber force field wherein intratube VDW interactions are treated taking the carbon atoms as uncharged Lennard-Jones particles with radii (σ_{C-C}) of 3.816 Å[25−33] and potential well depths (ϵ_{C-C}) of 0.086 kcal/mol.[26] To calculate the strain energies of SWNT rings versus radius, the geometry of the tube was relaxed by allowing stretching along both the tubular axis and radius directions. The calculated energies of the SWNT versus its radius are shown in Figure 2.

In our previous study,[13] the energy difference between a SWNT interacting with COOH- and CH_3-terminated surfaces was determined to be 0.04 kcal/mol per carbon atom. This energy difference matches the strain energy arising from a circular SWNT for a radius of 50 nm (Figure 2). Therefore, the minimum radius of a SWNT ring stable within the COOH-terminated feature is approximately 50 nm. This

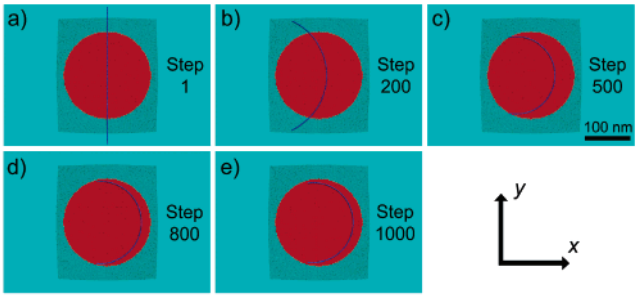

Figure 3. Monte Carlo simulation snapshots of the bending of a 314-nm-long (9,6) SWNT on the COOH- and CH_3-terminated templates at steps 1, 200, 500, 800, and 1000, respectively. Red and deep green colors represent the COOH- and CH_3-terminated SAMs, respectively, whereas the CH_3-terminated SAM with continuum model is shown in light green. The SWNT is shown in blue.

result is unlikely to change significantly with tube chirality because the number of carbon atoms in contact with the surface and the bending energy function are not expected to change significantly. For larger-diameter tubes, the strain energy in Figure 2 is expected to increase approximately linearly with tube diameter; however, the number of atoms also increases nearly linearly, so the radius where these two are equal should be about the same. A similar argument applies to longer tubes because both the energy in Figure 2 and the number of atoms increases linearly with tube length. The 50 nm estimate neglects the possibility of tube reconstruction (i.e., buckling) when the tube is bent. Such reconstruction would reduce the stress, yielding a smaller estimate for the radius.

To confirm this simple estimate, we simulate the bending of a SWNT on the molecular template. Using a recently developed parallel Monte Carlo program package, we were able to model at the atomic level the directed assembly of a 314-nm-long (9,6) SWNT on a 220 × 260 nm^2 molecular template (here taken to be the *xy* plane, as depicted in Figure 3). The template consists of a 100-nm-radius circle of COOH-terminated molecules surrounded by CH_3-terminated molecules (see the Supporting Information for the construction of the SWNT and the molecular templates). In the simulations, the template molecules are fixed. Initially, a linear SWNT was placed at the center of the circular molecular template and 0.75 nm above the surface, which is approximately the equilibrium distance. The *y* coordinate of the center of mass of the SWNT was fixed, but the tube was allowed to move freely in the *x* and *z* directions. Also, the tube is assumed to lie on a circular arc, with its curvature (1/*r*) randomly sampled. The maximum displacement allowed in each step was 50 Å and 5.0 × 10^{-5} Å along the *x* and *z* axes, respectively. The curvature is varied subject to a maximum change in each step of 2.5 × 10^{-3} $Å^{-1}$. The strain energy of the SWNT for different radii was obtained by interpolation from Figure 2, and the VDW energy is obtained by explicit summation over pair interactions subject to a 30 Å cutoff (the cutoff changes the VDW energy by only 0.3%). When the SWNT extends beyond the edge of the templated region, the interactions between that portion of the SWNT and the substrate is obtained by interpolation based on

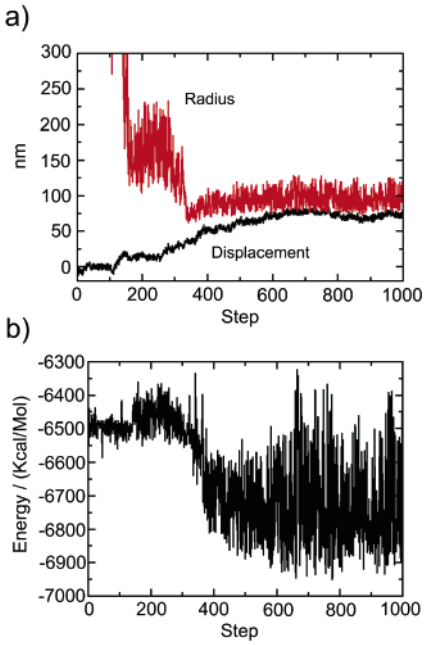

Figure 4. (a) Evolution of the radius and displacement along the *x* axis of the tube in Figure 3 as a function of step number. (b) Evolution of the energy of the system as a function of step number.

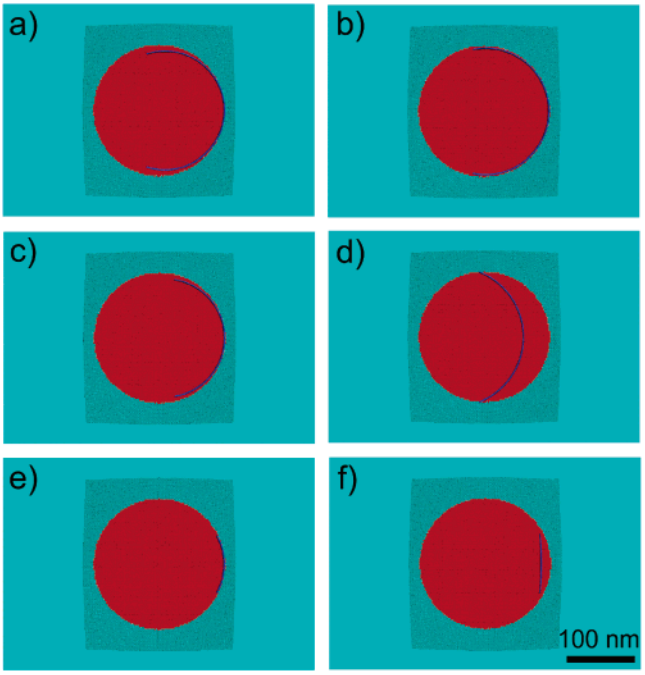

Figure 5. Length-dependent assembly of a (9,6) SWNT over the molecular template. (a and b) The initial and final state of a 340-nm-long SWNT. (c and d) The initial and final state of a 255-nm-long SWNT. (e and f) The initial and final state of a 90-nm-long SWNT.

interactions that were calculated separately between a purely CH_3-terminated SAM and the SWNT as a function of the distance between the SWNT and the surface.

Figure 3 shows snapshots of the formation of SWNT rings over the COOH- and CH_3-terminated SAMs. The simulation shows that the arc radii decrease gradually while the tube moves along the *x* axis toward the COOH/CH_3 boundary. This evolution is presented in Figure 4a, while Figure 4b shows the system energy. Initially, the radius decreases until reaching ~150 nm, where the displacement along *x* rises to a plateau at 15 nm. The corresponding snapshot (Figure 3b) shows a slightly curved SWNT with an increasing fraction of the tube in contact with the dot feature of COOH-terminated SAM. When the SWNT reaches a radius of ~150 nm, the system energy (Figure 4b) shows a small barrier that arises when the tube is bent without appreciably increasing the portion of the tube that is in contact with the COOH-terminated SAM. Then the energy decreases when the radius drops to 75 nm. This occurs when the SWNT has bent to the point where it overlaps strongly with the dot feature of the COOH-terminated SAM (going from Figure 3b to c). After this, the displacement of the SWNT grows slowly and reaches a plateau of ~80 nm after about 600 steps, where the SWNT ring stabilizes at a radius of 90 nm. This simulation is consistent with our estimate of the minimum radius given above.

In the above simulations, because of the large displacement and radius change of the SWNT at each step, the final state of the SWNT is still 20 nm away from the interface between the two-component molecular templates. To obtain a more precise configuration, we carried out simulations with smaller step sizes and different initial configurations. In these simulations, the substrate atoms are fixed as before. A 340-nm-long SWNT (3.4 times the COOH SAM feature radius) was placed near the COOH- and CH_3-terminated interface with a starting radius of 90 nm. Again, the SWNT was allowed to move along the *x* and *z* axes and bend correspondingly, but the maximum changes in curvature ($1/r$) and in the displacements along the *x* and *z* axes for each step were chosen to be 2.5×10^{-4} Å^{-1}, 5 Å, and 5.0×10^{-5} Å, respectively. The initial and final states of the simulations are shown in Figure 5a and b, respectively. A stable structure is found when the SWNT is only 1 nm away from the COOH- and CH_3-SAM boundary with a bending radius of 98 nm.

To further show how the assembly of SWNT rings depends on the relative length scales of the SWNTs and the molecular template, we perform calculations that start from the same initial state and with the same step size as for the 340 nm tube simulation, but using a 255-nm-long SWNT (Figure 5c). Minimization leads to a structure with a radius of 108 nm that is 40 nm away from the interface (Figure 5d). As the length decreases further, the SWNT gradually favors linear geometry. Figure 5e and f shows that for a 90-nm-long SWNT the tube remains nearly linear, lying 15 nm away from the starting place within the COOH template. This length dependence of the SWNT assembly arises from the balance between strain energy and VDW interaction difference between the SWNT and different SAMs, and what we infer from Figure 5 is that tubes that are more than roughly 3 times the radius, that is, half the circumference, in length will favor circular tubes, whereas those less than the diameter in length will favor linear tubes. These results refer to a COOH-terminated feature size having a 100 nm radius. Unfortunately it is not possible to simulate larger feature sizes, but we expect that the transition between circular tubes and linear tubes will still be governed by

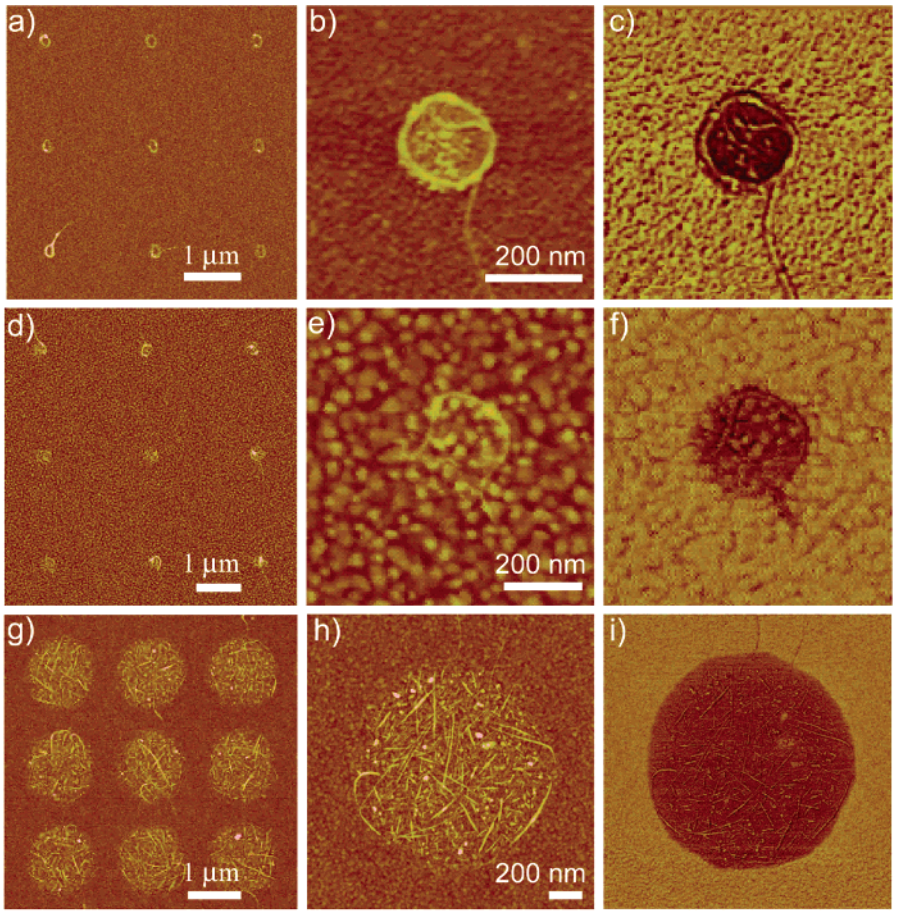

Figure 6. Length-dependent directed assembly of SWNT rings on MHA dots of different diameters: (a−c) 200 nm; (d−f) 350 nm; (g−i) 1.2 μm. c, f, and i are lateral force microscopy images and the rest are tapping-mode AFM topographic images. The images were taken at a scan rate of 0.5 Hz. The height scale is 20 nm, and the phase lag is 20°.

similar criteria. As long as the tube exhibits linear elastic behavior, with a bending modulus that is length-independent, the ratio of tube length to feature radius associated with this transition should stay the same.

The theoretical simulations are accurately confirmed by the experiments as shown in Figure 6. Simply by varying the MHA dot sizes or SWNT lengths with strategies similar to those used in earlier studies,[13] we fabricated SWNTs with three different structures, including (1) rings, when the SWNT is longer than the dot circumference (Figure 6a−c); (2) arcs, when the SWNT is shorter than the dot circumference but longer than the diameter of the dot (Figure 6d−f); and (3) straight tubes, when the SWNTs are shorter than the diameter of the MHA dots (Figure 6g−i). Although the comparison between theory and experiment depends on the assumptions noted above about the influence of feature size, tube length, tube diameter, and absence of buckling, and it also implicitly assumes that the experiment results are controlled by thermodynamic rather than kinetic effects, the agreement is very good.

We note that this length dependence may also be influenced by the solvent dewetting kinetics on a larger length scale, as others have observed for a different system (surfactant-dispersed SWNTs in water).[20] However, for the 1,2-dichlorobenzene solvent used for this study, bent SWNT structures were rarely observed on the SAMs we have explored other than COOH-terminated SAMs.[13] For feature sizes between micrometers and the bulk, it is not clear that complex dewetting behavior can become dominant in driving tube bending.

In conclusion, we have presented a quantitative comparison between experiment and theory on the formation of SWNT rings on a surface using molecular templates. By adapting a Monte Carlo method, our algorithm allows modeling of the assembly process for large systems at the atomic level. As the simulations predicted, SWNTs were assembled over MHA dots, forming rings with a radius as small as 100 nm. Attempts to produce smaller ring structures were not successful. Thus, we see that the formation of SWNT rings is driven by the balance between the strain arising from tube bending and the differences in VDW interactions with the molecular templates. This work, together with our previous report,[13] provides a comprehensive model for the surface assembly/manipulation of these nanoscale building blocks.

Acknowledgment. G.C.S. and S.Z. acknowledge the NASA BIMAT Center at Northwestern and NSF for support of this research. C.A.M. acknowledges the AFOSR, ARO, DARPA, NIH, and NSF for support of this work. C.A.M. is also grateful for a NIH Director's Pioneer Award. D.M. acknowledges the Generalitat de Catalunya for a postdoctoral grant.

Supporting Information Available: Detailed experimental procedures and a description of the parallel program package and the SWNT and molecular template models. This material is available free of charge via the Internet at http://pubs.acs.org.

References

(1) Jenekhe, S. A.; Chen, X. L. *Science* **1999**, *283*, 372−375.
(2) Seeman, N. C. *Nature* **2003**, *421*, 427−431.
(3) Yan, H.; Park, S. H.; Finkelstein, G.; Reif, J. H.; Labean, T. H. *Science* **2003**, *301*, 1882−1884.
(4) Percec, V.; Glodde, M.; Bera, T. K.; Miura, Y.; Shiyanovskaya, I.; Singer, K. D.; Balagurusamy, V. S. K.; Heiney, P. A.; Schinell, I.; Papp, A.; Spiess, H. W.; Hudson, S. D.; Duan, H. *Nature* **2002**, *419*, 384−387.
(5) Adleman, L. M. *Science* **1994**, *266*, 1021−1024.
(6) Braich, R. S.; Chelyapov, N.; Johnson, C.; Rothemund, P. W. K.; Adleman, L. *Science* **2002**, *296*, 499−502.
(7) Service, R. F. *Science* **2005**, *309*, 95−95.
(8) Goldhaber-Gordon, D.; Montemerlo, M. S.; Love, J. C.; Opiteck, G. J.; Ellenbogen, J. C. *Proc. IEEE* **1997**, *85*, 521−540.
(9) Heath, J. R.; Ratner, M. A. *Phys. Today* **2003**, *5*, 43−49.
(10) Nitzan, A.; Ratner, M. A. *Science* **2003**, *300*, 1384−1389.
(11) Reed, M. A.; Lee, T. *Molecular Nanoelectronics*; American Scientific Publishers: Stevenson Ranch, CA, 2003.
(12) Whitesides, G. M.; Grzybowski, B. *Science* **2002**, *295*, 2418−2421.
(13) Wang, Y.; Maspoch, D.; Zou, S.; Schatz, G. C.; Smalley, R. E.; Mirkin, C. A. *Proc. Natl. Acad. Sci. U.S.A.* **2006**, *103*, 2026−2031.
(14) Ginger, D. S.; Zhang, H.; Mirkin, C. A. *Angew. Chem., Int. Ed.* **2003**, *43*, 30−45.
(15) Piner, R. D.; Zhu, J.; Xu, F.; Hong, S.; Mirkin, C. A. *Science* **1999**, *283*, 661−663.
(16) Liu, J.; Dai, H.; Hafner, J. H.; Colbert, D. T.; Smalley, R. E.; Trans, S. J.; Dekker, C. *Nature* **1997**, *385*, 780−781.
(17) Martel, R.; Shea, H. R.; Avouris, P. *Nature* **1999**, *398*, 299.
(18) Yakobson, B. I.; Avouris, P. *Appl. Phys.* **2001**, *80*, 287−327.
(19) Sano, M.; Kamino, A.; Okamura, J.; Shinkai, S. *Science* **2001**, *293*, 1299−1301.
(20) Tsukruk, V. V.; Ko, H.; Peleshanko, S. *Phys. Rev. Lett.* **2004**, *92*, 065502.
(21) Song, L.; Ci, L.; Sun, L. C. J.; Liu, L.; Ma, W. D. L.; Zhao, X.; Luo, S.; Zhang, Z.; Xiang, Y.; Zhou, J.; Zhou, W.; Ding, Y.; Wang, Z.; Xie, S. *Adv. Mater.* **2006**, *18*, 1817−1821.
(22) Shea, H. R.; Martel, R.; Avouris, P. *Phys. Rev. Lett.* **2000**, *84*, 4441−4444.
(23) Liu, J.; Casavant, M. J.; Cox, M.; Walters, D. A.; Boul, P.; Lu, W.; Rimberg, A. J.; Smith, K. A.; Colbert, D. T.; Smalley, R. E. *Chem. Phys. Lett.* **1999**, *303*, 125−129.
(24) Rao, S. G.; Huang, L.; Setyawan, W.; Hong, S. *Nature* **2003**, *425*, 36−37.
(25) Lu, J. P. *Phys. Rev. Lett.* **1997**, *79*, 1297−1300.
(26) Girifalco, L. A.; Hodak, M.; Lee, R. S. *Phys. Rev. B* **2000**, *62*, 13104−13110.
(27) Tersoff, J.; Ruoff, R. S. *Phys. Rev. Lett.* **1994**, *73*, 676−679.
(28) Che, J.; Cagin, T.; Goddard, W. A., III *Nanotech.* **1999**, *10*, 263−268.
(29) Hummer, G.; Rasaiah, J. C.; Noworyta, J. P. *Nature* **2001**, *414*, 188−190.
(30) Zhu, F.; Schulten, K. *Biophys. J.* **2003**, *85*, 236−244.
(31) Walther, J. H.; Jaffe, R.; Halicioglu, T.; Koumoutsakos, P. *J. Phys. Chem. B* **2001**, *105*, 9980−9987.
(32) Gao, H.; Kong, Y. *Annu. Rev. Mater. Res.* **2004**, *34*, 123−150.
(33) Lu, G.; Maragakis, P.; Kaxiras, E. *Nano Lett.* **2005**, *5*, 897−900.

NL062258E